Thin films of lamellar forming polydisperse di-block copolymers

Rajeev Kumar,[*,†,‡] Bradley S. Lokitz,[¶] Scott W. Sides,[§] Jihua Chen,[¶] William Heller,[‖] John F. Ankner,[‖] Jim Browning,[‖] S. Michael Kilbey II,[⊥] and Bobby G. Sumpter[¶]

Computer Science and Mathematics Division, Oak Ridge National Lab, Oak Ridge, TN-37831, Center for Nanophase Materials Sciences, Oak Ridge National Lab, Oak Ridge, TN-37831, Center for Nanophase Materials Sciences,Oak Ridge National Laboratory, Oak Ridge, TN-37831, National Renewable Energy Laboratory, Golden, CO-80401, Spallation Neutron Source, Oak Ridge National Laboratory, Oak Ridge, TN-37831, and Department of Chemistry, University of Tennessee, Knoxville, TN-37996

E-mail: kumarr@ornl.gov

Abstract

Microphase separation in thin films of lamellar forming polydisperse di-block copolymers is studied using self-consistent field theory (SCFT) and neutron reflectivity experiments. Di-block copolymers containing a polydisperse block (poly(glycidylmethacrylate) (PGMA)) connected to a near monodisperse block (poly(4,4-dimethyl-d6-2-vinylazlactone) (PVDMA-d_6))

[*]To whom correspondence should be addressed
[†]Computer Science and Mathematics Division, Oak Ridge National Lab, Oak Ridge, TN-37831
[‡]Center for Nanophase Materials Sciences, Oak Ridge National Lab, Oak Ridge, TN-37831
[¶]Center for Nanophase Materials Sciences,Oak Ridge National Laboratory, Oak Ridge, TN-37831
[§]National Renewable Energy Laboratory, Golden, CO-80401
[‖]Spallation Neutron Source, Oak Ridge National Laboratory, Oak Ridge, TN-37831
[⊥]Department of Chemistry, University of Tennessee, Knoxville, TN-37996

are considered in this work. Effects of chain length polydispersity, film thickness, substrate-monomer and monomer-monomer interactions on the microphase segregation are studied using SCFT. The theoretical study reveals that an increase in polydispersity tends to decrease the number of lamellar strata that can be packed in a film of given thickness, in comparison to a film created with monodisperse di-block copolymers. This is a direct consequence of an increase in lamellar domain spacing with an increase in polydispersity index. These predictions are verified by comparison with neutron reflectity experiments done on thin films made from moderately polydisperse PGMA-b-PVDMA-d_6 di-block copolymer deposited on silicon substrates. Furthermore, it is shown that polydispersity induces conformational asymmetry and an increase in the polydispersity index makes the polydisperse blocks less flexible in comparison with monodisperse blocks. It is shown that conformational asymmetry effects, which are entropic in origin and of increasing importance as film thickness descreases, drive the polydisperse blocks to the middle of the films despite favorable substrate interactions. Prediction of neutron reflectivity profiles using the SCFT provides a facile and robust route for model verification and leads to useful physical insights into behavior of di-block copolymers near interfaces.

Almost all polymers are polydisperse.[1] Understanding the effects of chain length polydispersity on structure and self-assembly has been one of the most important problems in polymer physics.[2–18] Most theoretical studies[19,20] deal with monodisperse polymers and copolymers, rather than polydisperse systems, due to relative ease of modeling such systems. Demonstration of the facts that even polydisperse block copolymers can self-assemble into well-ordered morphologies[7–15] and macrophase separation[7,8] in these systems has led to a renewed interest in understanding effects of polydispersity in block copolymers.

Self-consistent field theory[3–5,7,8] (SCFT) and Monte-Carlo (MC) simulations[9,11] have been used to study micro as well as macro phase separation in di-block copolymer melts containing one polydisperse block connected to a monodisperse block. Predictions of the theory are compared with experiments[8] on similar systems and despite some unresolved issues that occur near the disorder-order transition temperature, reasonable agreement between the SCFT predictions,

MC simulations and experiments are found. However, effects of chain length polydispersity on microphase separation in thin films are not widely studied and still pose a challenge to the scientific community.

On the experimental side, specular neutron reflectivity[21–26] provides very useful insights into structure of thin films normal to the substrate. However, interpretation of the reflectivity curves requires modeling scattering length density (SLD) (number of nuclei per unit area) profiles. SLD depends on the relative volume fractions of the constituent monomers of a blend. For the lamellar forming polydisperse di-block copolymers studied in this work, *a priori* it is not clear how to set up the gross features of the SLD profiles due to a lack of knowledge about the number of lamellar strata that can be accomodated in a film of a given thickness. The SCFT can be used as a complementary tool to predict the number of lamellar strata that can be packed in a film, whose thickness is determined from fringes in neutron reflectivity or using other techniques like ellipsometry. Furthermore, the density profiles obtained from the SCFT can be used to construct the SLD profiles and neutron reflectivity curves for a direct comparison with experiments.

In this work, our focus is to study microphase separation in thin films of lamellar forming polydisperse di-block copolymers, where one block is polydisperse and the other is nearly momnodisperse. This work is motivated by two goals. First goal is to develop of a fundamental understanding of the effects of polydispersity in chain lengths on the microphase separation in thin films, which is different from the separation in bulk. Second goal is to develop a computational framework for the prediction of neutron reflectivity profiles for the thin films and verify some of the theoretical predictions. For such purposes, we have generalized the SCFT[27] for polydisperse di-block copolymer melts to thin films. Using the theory, we have studied the effects due to the strengths of monomer-monomer and substrate-monomer interactions, film thickness and polydispersity on the microphase separation. Analytical treatment of polydisperse di-block copolymer melts in the strong segregation limit as well as numerical SCFT are used to demonstrate polydispersity-induced conformational asymmetry[28,29] and study its implications on microphase separation in thin films.

Also, we have synthesized poly(glycidylmethacrylate)-b-poly(4,4-dimethyl-d6-2-vinylazlactone

(PGMA-b-PVDMA-d_6) di-block copolymers so that the PGMA blocks are polydisperse and the PVDMA-d_6 blocks are narrowly-dispersed. Our interest in studying PGMA-b-PVDMA-d_6 di-block copolymers lies in the use of these polymers for the creation of functional polymers and surfaces due to the reactive polymer poly(vinyl dimethyl azlactone) (PVDMA). Microphase segregation in the bulk as well as in thin films containing these polymers is studied using small angle neutron scattering (SANS), transmission electron microscope (TEM) and neutron reflectivity (NR) experiments. The NR experiments provide a unique opportunity for non-invasive monitoring of the layer segment density profile. In order to create scattering contrast between the two blocks, VDMA-d_6 was synthesized and used in these studies. Deuterium substitution of the protons on the dimethyl groups of the azlactone ring increases the scattering length density (SLD) by a factor of 2.75 over that of VDMA, allowing for the construction of a neutron reflectivity model to represent the experimental data. Density profiles computed via the SCFT are used to construct scattering length density (SLD) profiles as well as neutron reflectity profiles. These profiles are compared with experiments done on the PGMA-b-PVDMA-d_6 copolymer films.

Results and Discussion

In order to develop a fundamental understanding of microphase separation in thin films of polydisperse di-block copolymers, we have simulated films of varying thicknesses containing polymers of different PDIs. The theoretical predictions and comparison between theory and experiments are sequentially presented in the following sections.

Theoretical predictions

Annealing the thin polymer films provides mobility to the chains, and also allows the epoxide groups of PGMA to react with silenol groups on the silicon substrate. This reaction secures di-block copolymer chains to the substrate. Also, it has been shown that PVDMA-d_6 tends to prefer the air interface.[30] Keeping this in mind, we have studied a polydisperse $A-B$ block copolymer

system where the polydisperse block has a preference for one substrate and dislikes the other.

Such an asymmetry in interactions leads to volume fraction profiles as shown in Figure 1, where the components A and B have preference for left and right substrate, respectively. The asymmetry in interactions leads to higher volume fraction of component A next to the left substrate in Figure 1 and depletion from the right. In our simulations, we take into account diffuse nature of the two substrates by incorporating masking functions (cf. Figure 1). These functions are assumed to be known e.g., from modeling of neutron reflectivity data. In this section, we have taken these masking functions to be of the form $0.5(1 \pm \tanh((z - z_{\pm})/\xi_{\pm}))$, where $+$ and $-$ corresponds to polymer-air and polymer-silicon interface, respectively. Parameters $z_{\pm}$ and $\xi_{\pm}$ prescribe the centre and width of the masking functions, respectively.

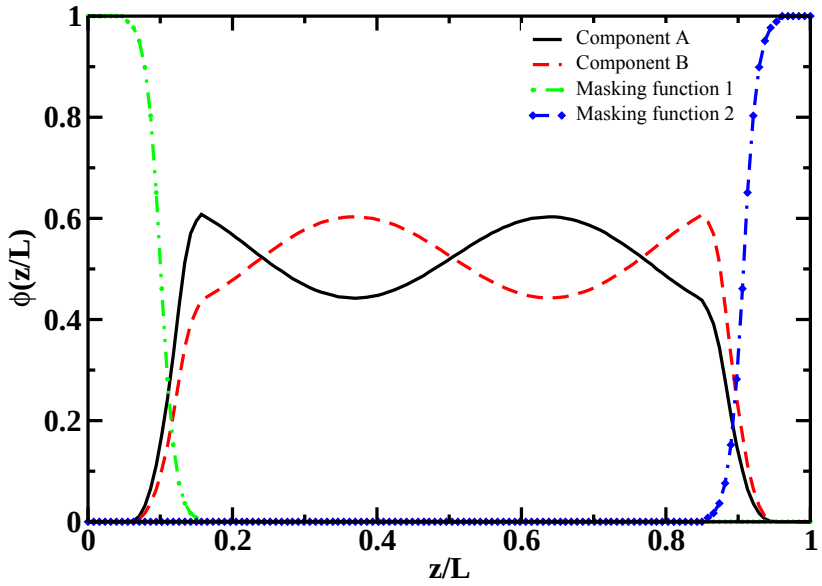

Figure 1: Volume fraction profiles of different components and masking functions used to simulate structure in thin films of 50 : 50 di-block copolymers.

We have parameterized interaction energy between the monomers and particles in the substrates by χ parameters. Subscripts t, b are used to represent air ("top") and silicon ("bottom") substrate, respectively. For example, χ_{tA} represents the parameter for interaction between A monomer species and the air. The interaction parameters χ_{jA} and χ_{jB} $(j = t, b)$ determine tendencies for the polymer

chains to either wet or be excluded from the confining surface. The relative sizes of the χ parameters determine the effective attraction or replusion for a monomer species to a substrate species. For example, if $\chi_{tA} < \chi_{tB}$ then A monomers preferentially wet the substrate. Absolute values of these parameters determine how strongly the monomers are repelled from the substrates.

We have systematically varied different parameters to study their effect on structure in the thin films. We have found that the polydispersity of the A block leads to two effects. First, in strongly confined systems corresponding to film thicknesses (L) less than $6R_g$, R_g being the radius of gyration of Gaussian chains of the same length as investigated, the polydisperse block tends to populate the middle of the film despite favorable interactions of the block with one of the substrates (cf. Figure 2). Second, in weakly confined systems so that $L > 6R_g$, an increase in segregation strength is observed with an increase in PDI_A (cf. Figure 3). This leads to dependence of the number of strata that can be packed in a given film on the polydispersity index (cf. Figure 4). Both of these effects play important roles in the modeling and interpretation of neutron reflectivity data as discussed in the next section.

In order to investigate origin of the first effect, we have increased PDI_A and found an an increase in volume fraction of the polydisperse component near the middle of the film as shown in Figure 2(a) and depletion from the substrate with preferential interactions. Also, we have varied the interaction energy parameter between the polydisperse block and the left substrate for the thinnest films, and results are presented in Figure 2(b). An increase in the interaction energy parameter between the polydisperse block and the left substrate leads to an increase in volume fraction next to the substrate. The observed behavior in the thin films of polydisperse di-block copolymer system is quite similar to entropic effects at play in a confined polymer blends resulting from conformational asymmetry between the polymers constituting the blend. In particular, it has been shown[31] that in a binary blend, the polymer having a smaller Kuhn segment length tends to prefer the substrate in cases where interaction energies with substrates are negligible. Furthermore, entropic effects are shown to be strongest in the thinnest films. This is in striking qualitative agreement with the thin films of polydisperse di-block copolymers where such behavior is observed in

films of thickness $L < 6R_g$, R_g being the radius of gyration of the chains in the absence of any interactions. An increase in the interaction energy parameter between the polydisperse block and the left substrate is similar to transition from an entropy dominated regime to energy dominated regime (cf. Figure 2(b)). Using this analogy, it appears that chains in the polydisperse block have h

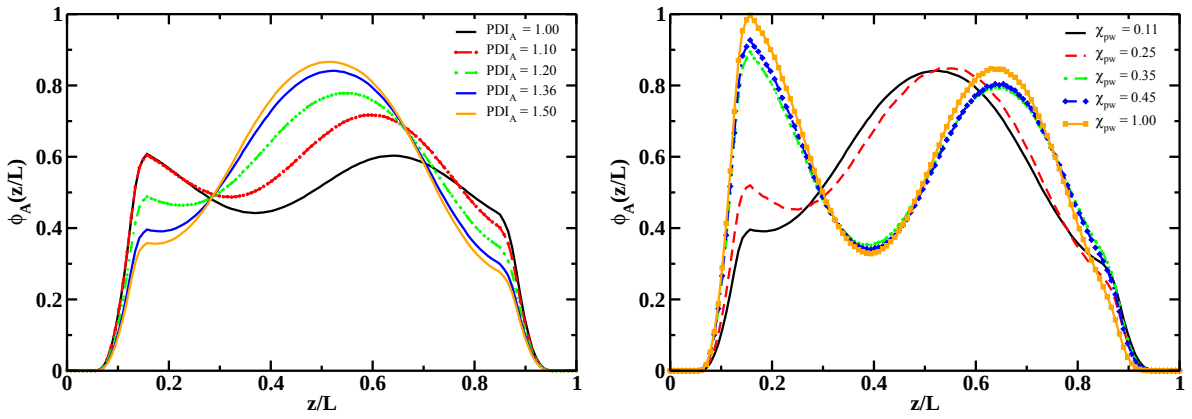

(a) (b)

Figure 2: Effects of polydispersity and polymer-substrate interaction strength on the microphase segregation in a film of thickness $L/R_g = 5$ is shown here. In Figure (a), the polydisperse component populates the middle of the film despite favorable interactions ($\chi_{At} = \chi_{Bb} = 0.11$) with one of the substrates (corresponding to $z = 0$ in Figure (a)). An increase in polymer-substrate interaction parameter (so that $\chi_{At} = \chi_{Bb} = \chi_{pw}$) leads to enrichment of the polydisperse component near the substrate with favorable interaction parameter. For both of these figures, we have taken $\chi_{AB}N = 10, \chi_{Ab} = \chi_{Bt} = 0.001$ and $\mathrm{PDI}_A = 1.36$.

Insights into the effects of PDI on the conformational entropy and in turn, on the "effective" Kuhn segment length can be obtained by considering the strong stretching limit. In this limit, the chain conformational entropy in a lamellar morphology can be approximated by the cost of stretching (per chain) a polydisperse brush[6,32] by a distance D, given by

$$\frac{F_{st}}{nk_BT} = \frac{\pi^2 D^2}{32\langle N\rangle_n}\left[\frac{f_A S_A}{l_A^2} + \frac{(1-f_A)}{l_B^2}\right] \tag{1}$$

where f_A is the volume fraction of A component, $\langle N\rangle_n$ is the number average molecular weight of

the chains and

$$S_A = \int_0^\infty dN \left[1 - \int_0^N dN' p_A(N')\right]^3 \leq 1 \tag{2}$$

Numerical estimates of S_A can be obtained assuming that the chain-length of the A block are distributed as

$$p_A(N) = \left(\frac{N}{N_A}\right)^{\nu-1} \frac{\exp\left[-N/N_A\right]}{N_A \Gamma(\nu)} \tag{3}$$

For the distribution, the number average, weight average and polydispersity index of A block is given by $\langle N_A \rangle_n = \nu N_A, \langle N_A \rangle_w = (\nu+1) N_A$ and $\mathrm{PDI}_A = (\nu+1)/\nu$, respectively. This, in turn, leads to the number average molecular weight of the *chains* as $\langle N \rangle_n = \nu N_A + N_B$ Numerical calculations based on the Schulz-Zimm distribution reveal that S_A decreases with increasing PDI_A. Physically, this means that it is easier to stretch the polydisperse system in comparison with the monodisperse. From Eq. 1, we can define an "effective" Kuhn segment length of the polydisperse chains as $l_{A,eff} = l_A/\sqrt{S_A} > l_A$. Numerical evaluations[6] of S_A reveals that it decreases monotonically with an increase in PDI_A. This, in turn, leads to an increase in the effective Kuhn segment length. Such an effect of the polydispersity leads to induction of conformational asymmetry even in near symmetric systems and leads to the entropic effects in the thin films as discussed above.

Effects of the chain length polydispersity on the conformational entropy also manifest as an increase in domain spacing in the bulk (i.e., without any substrates) with increasing PDI. Adding the conformational entropy (Eq. 1) to the interfacial energy of a planar interface in the strong segregation limit, the domain spacing of a lamella formed by the polydisperse $A-B$ di-block copolymers is given by

$$D = D_0 \left[f_A S_A + (1 - f_A)\right]^{-1/3} \tag{4}$$

where $D_0 = 2\left[\frac{8\chi_{AB}\langle N \rangle_n}{3\pi^4}\right]^{1/6} \langle N \rangle_n^{1/2} l$. Noting that $S_A = 1$ for $\mathrm{PDI}_A = 1$, $D \to D_0$ becomes the domain

spacing adopted by a melt of monodisperse $A-B$ di-block copolymers. In writing Eq. 4, we have ignored the conformational asymmetry of the two blocks i.e., $l_A = l_B = l$. As $f_A < 1, S_A < 1$, it is clear from Eq. 4 that $D > D_0$. In other words, the domain spacing of the lamellar morphology increases with an increase in PDI_A due to decrease in S_A. Numerical estimates of the changes in domain spacing in the strong segregaton limit resulting from Eq. 4 are shown in Figure 3(a). Also, volume fraction profiles from the SCFT calculations for $L = 12R_g$ in the weak segregation limit ($\chi_{AB}N = 10$) for different values of PDI_A are shown in Figure 3(b). Numerical results for volume fraction profiles show that sharper interfaces are formed with an increase in PDI_A without any significant changes in the domain spacing. Figure 3 highlights different effects of polydispersity on the microphase segregation in the bulk and thin films. In the latter, confinement effects also play an important role. The confinement and polymer-substrate interaction effects are also responsible for the observed order in films even when $\chi_{AB}N < 10$ (cf. Figure 4(a)) where no such order is found in the bulk (note that $\chi_{AB}N = 10.495$ for disorder-order transition in the melts of monodisperse di-block copolymers).

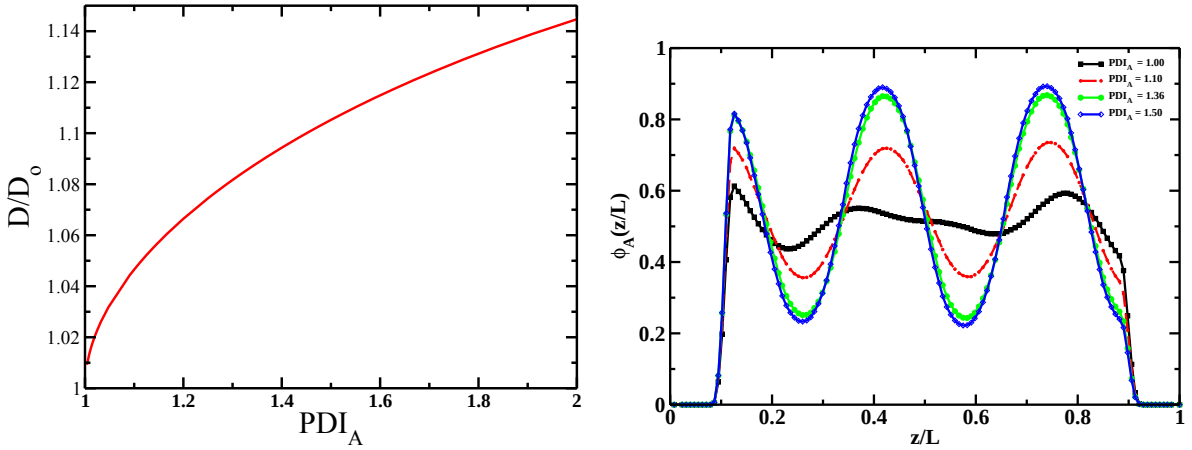

(a) (b)

Figure 3: Effect of PDI on the microphase segregation strength is shown here for the bulk and thin films. Figure (a) shows the theoretical predictions (cf. Eq. 4) for domain spacing of lamella morphology in polydisperse di-block copolymer melts (without any boundaries) so that one block is polydisperse and the other is monodisperse. Figure (b) shows SCFT predictions for the volume fraction profiles of the polydisperse block in a film of thickness $L/R_g = 12, \chi_{AB}N = 10, \chi_{Ab} = \chi_{Bt} = 0.001, \chi_{At} = \chi_{Bb} = 0.11$ and $\text{PDI}_A = 1.36$.

Conformational entropy also has an important role in dictating the number of strata that can be packed in a film of known thickness. For monodisperse di-block copolymers, work by Turner[33] in the strong segregation limit has shown that the ratio of film thickness (L) to the domain spacing of the lamellae in the absence of substrates (D) is one of the key parameters, which dictates the number of layers that can be packed in a given film. One of the predictions of the theory is an increase in the number of strata with an increase in L/D in discrete (quantized) steps. Hence, with an increase in the PDI, the number of strata that can be packed in a film of known thickness should decrease due to increase in D (cf. Figure 3) and quantization of the ratio L/D as per Ref.[33] Note that the theory is strictly valid in the strong segregation limit ($\chi_{AB}N \to \infty$) and our numerical computations are done in the weak and intermediate segregation limit (i.e., $\chi_{AB}N < 50$) due to their relevance for experimental data presented in the next section. Despite these differences in the segregation strengths, we see qualitative agreement between the theory and the SCFT results in Figure 4, where we compare volume fraction profiles of monodisperse and polydisperse di-block copolymers in thin films. It can be seen that the thin film of thickness $L = 10R_g$ has three peaks in the volume fraction profile for the monodiserse case whereas the volume fraction profile for the $\mathrm{PDI}_A = 1.36$ has only two peaks. This is in agreement with the prediction of decrease in the number of strata that can be packed in a film of known thickness with an increase in the PDI. However, for $L = 5R_g$, volume fraction profiles are significantly different even in qualitative features due to the entropic effects discussed above.

These effects of the polydispersity on the volume fraction profiles in the polymer thin films can be verified and at the same time, aid in interpretting neutron reflectivity data. In the next section, we compare results of the SCFT modeling of the thin films with those from neutron reflectivity experiments on PGMA-b-PVDMA-d_6 block copolymer.

Comparison with neutron reflectivity experiments

Our numerical results show that polydispersity can have different effects on different characteristics of the microphase separation in the bulk and the thin films (cf. Figure 3). Keeping this in mind, we

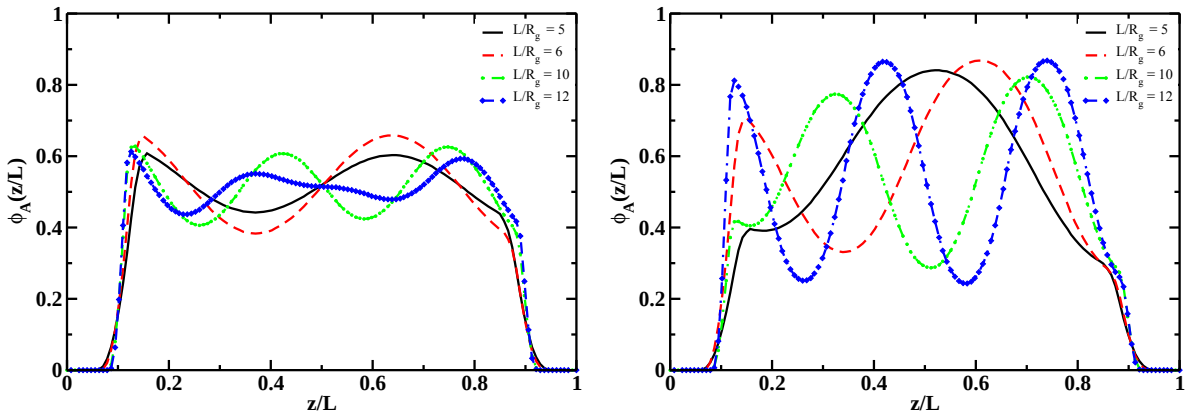

(a) (b)

Figure 4: Volume fraction profiles of the polydisperse component in thin films of 50 : 50 di-block copolymers for $\chi_{AB}N = 10, \chi_{Ab} = \chi_{Bt} = 0.001, \chi_{At} = \chi_{Bb} = 0.11$. Figure (a) represents films containing monodisperse chains and (b) correspond to films containing polydisperse block copolymers with $\mathrm{PDI}_A = 1.36$.

have done experiments to characterize microphase separation in the bulk as well as thin films. We syntesized di-block copolymers containing a polydisperse PGMA and narrowly dispersed PVDMA using reversible addition chain-transfer (RAFT) polymerization. Molecular characteristics of these polymers are presented in Table 1.

Table 1: Compositional and Molecular Weight Characteristics

Sample	Mol %	Mn[b] (kg/mol)	PDI[b]
PGMA MacroCTA	-	20.2	1.36
PGMA_{142}-b-PVDMA_{148}	50 %	40.8	1.19

a. Determined by ^{1}H NMR
b. Obtained from SEC-MALLS

The di-block copolymer was synthesized by chain extension of a PGMA macro-chain transfer agent (PGMA macroCTA), which had a PDI of 1.36. This, in turn, means that the PDI of the PGMA blocks in the di-block copolymers is 1.36. Furthermore, chain extension leading to the PGMA_{142}-b-PVDMA_{148} containing on an average 142 and 148 repeats of PGMA and PVDMA had a PDI of 1.19. Assuming that PVDMA is monodisperse and PGMA is distributed as per the

Schultz-Zimm distribution, PDI of the chain is given by[4]

$$\mathrm{PDI}_{PGMA-b-PVDMA} = \frac{(1+1/\nu)\langle N_{PGMA}\rangle^2 + 2\langle N_{PGMA}\rangle N_{PVDMA} + N_{PVDMA}^2}{[\langle N_{PGMA}\rangle + N_{PVDMA}]^2} \quad (5)$$

where $\mathrm{PDI}_{PGMA} = (\nu+1)/\nu$, $\langle N_{PGMA}\rangle$ is the number average of repeats in the PGMA blocks and N_{PVDMA} is the number of repeats in the PVDMA blocks. Here, we have used the approximation that GMA and VDMA monomer has equal molecular weight (~ 142 and ~ 139 for GMA and VDMA). For $\mathrm{PDI}_{PGMA} = 1.36$ (i.e., $\nu = 2.777$) as per Table 1 and taking $\langle N_{PGMA}\rangle = N_{PVDMA}$, Eq. 5 gives $\mathrm{PDI}_{PGMA-b-PVDMA} = 1.09$. This analysis shows that the PVDMA is not strictly monodisperse but has a narrow polydispersity. In our theoretical analysis, we assume that the PVDMA is monodisperse and PGMA has a PDI of 1.36. In future, we plan to extend the SCFT study to di-block copolymers where both blocks are polydisperse.

In order to quantify the segregation limit and morphology for the PGMA-b-PVDMAd_6 in the bulk (i.e., in the absence of substrates), we used SANS and TEM. Results of these characterizations are presented in Figure 5. The TEM image shows that morphology obtained in the bulk is lamellar. Also, the SANS data and fit for the first peak are shown in Figure 5. Based on the location of the peak, the domain spacing of the lamellar morphology is estimated to be 25.8 nm. Furthermore, using Eq. 4, $\chi_{PGMA-PVDMA-d_6}N = 120.62$, which reveals that the polydisperse block copolymer system lies in the strong segregation limit. Note that despite such a high value of $\chi_{PGMA-PVDMA-d_6}N$ long range order is not observed in the bulk as evident from the TEM image and absence of higher order peaks. This may be due to effects of PDI in driving the macrophase as well as microphase segregation.

In order to study microphase segregation in thin films, we have done neutron reflectivity experiments on three films of different thicknesses (45 nm, 34 nm and 15 nm as determined by modeling of neutron reflectivity data) spanning strongly confined to weakly confined regime for the chains. Results of these experiments and the best fits obtained for model SLD profiles are presented in Figure 6. For predicting neutron reflectivity profiles and comparing with the SCFT predictions,

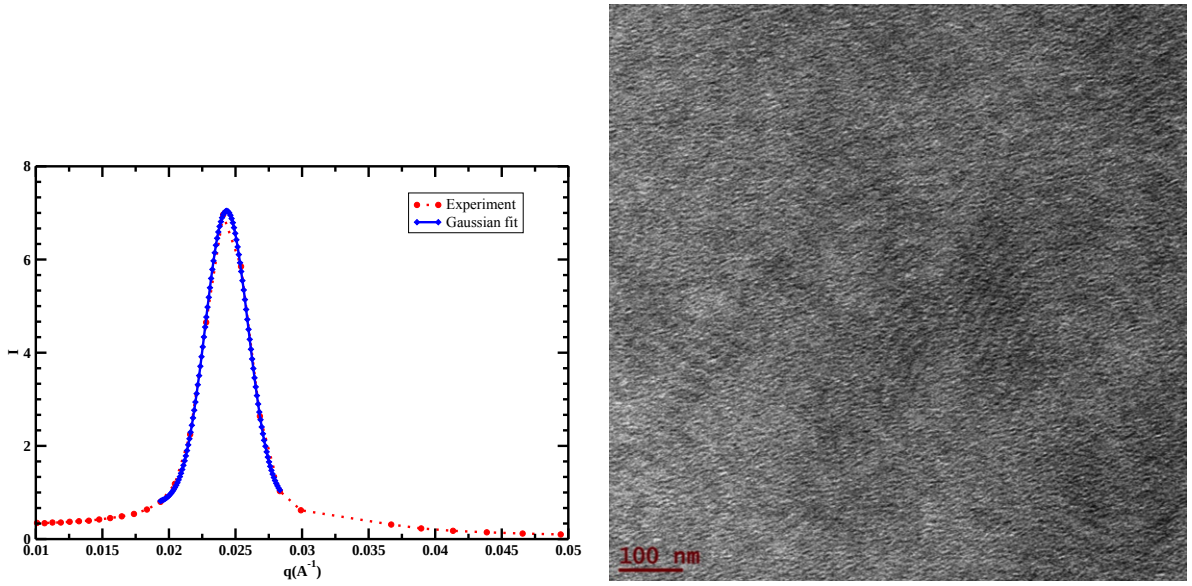

(a) (b)

Figure 5: SANS data (a) and TEM image (b) for the melts containing PGMA-GMA-PVDMA-d_6 di-block copolymers, showing lamellar morphology.

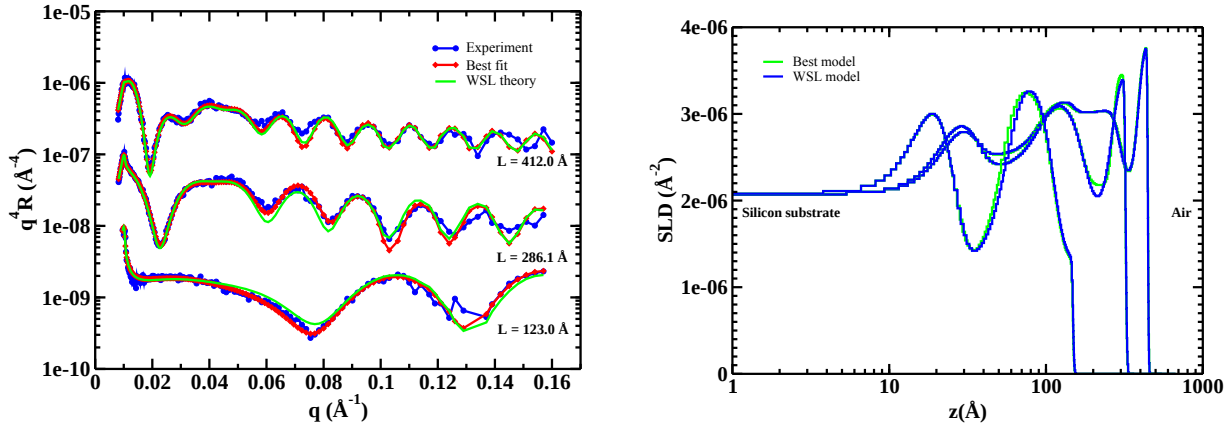

(a) (b)

Figure 6: Modeling of neutron reflectivity profiles for three films of PGMA-PVDMA-d_6 di-block copolymers. Top, middle and bottom figures correspond to films with total thicknesses of 45, 34 and 15 nm, respectively.

we have followed a three step procedure. In the first step, an initial estimate for the film thickness was obtained using fringes in the neutron reflectivity data. For these film thicknesses, the SCFT simulations with the hyperbolic tangent masking functions (as discussed in the previous section) were used to determine the number of strata that can be packed. These simulations were run to mimic PGMA-b-PVDMA-d_6 systems with $\mathrm{PDI}_{PGMA} = 1.36$ and different values of χ parameters characterizing polymer-polymer and polymer-substrate interactions. In the second step, a multi-layer model based on the number of strata was constructed to fit the neutron reflectivity data using Parratt's formalism. The best fits obtained using this protocol are shown in Figure 6. These fits were used to refine the thickness and masking functions for the simulations. In the third step, refined thicknesses and masking functions were used in the simulations. χ parameters were varied to change the volume fraction profiles inside the film. In order to obtain the volume fraction profiles from the SLD profiles for the best fits, we used the relation $SLD(\mathbf{r}) = \sum_{k=GMA,VDMA-d_6} SLD_k \phi_k(\mathbf{r})$, where SLD_k and ϕ_k represent SLD and volume fraction of the monomer of type k, respectively. Monomeric SLDs were computed using the molecular formula and density. Volume fraction profiles obtained in this way representing the best fits for the neutron reflectivity data are shown in Fig. Figure 7. Furthermore, reference density ρ_0 is computed from these volume fraction profiles by using the constraint that spatial average of volume fraction profiles must be 0.5, as per the chemical characterization presented in Table 1. Reults for the reference densities for different film thicknesses are presented in Fig. Figure 7(d).

These volume fraction profiles are compared with the predictions of analytical theory[34] in the weak segregation theory and results of such comparisons are presented in the Supporting Information. From these comparisons, we have estimated the $\chi_{PGMA-PVDMAd_6} \langle N \rangle_n$, which characterizes the segregation strength in the three films. These estimates are presented in Fig. Figure 7(d), which is in agreement with the fact that $\chi_{PGMA-PVDMAd_6} \sim 1/\rho_0$. These parameters were used along with refined film thicknesses and masking functions as input in the "refined" SCFT simulations. We have varied the χ parameters around the estimated value from the analytical theory and computed the volume fraction profiles. Results from these SCFT simulations are compared with

the volume fraction profiles presented in Fig. Figure 7(cf. Fig. Figure 8). From Figure 8, it is clear that the SCFT captures qualitative features and quantiative agreement with the experiments can be achieved by varying χ_{AB}, χ_{jA} and χ_{jB} parameters. The SCFT provides a physics-based platform for interpretting neutron reflectivity data. Note that in the absence of such a physics-based tool, interpretation of neutron reflectivity data relies on phenomenological inferences and fitting protocols. Thus, not only does the comparison of the SCFT-predicted density profiles with neutron reflectivity serve to validate the SCFT model, but it also provides a platform for interpreting neutron reflectivity data in an unambiguous manner.

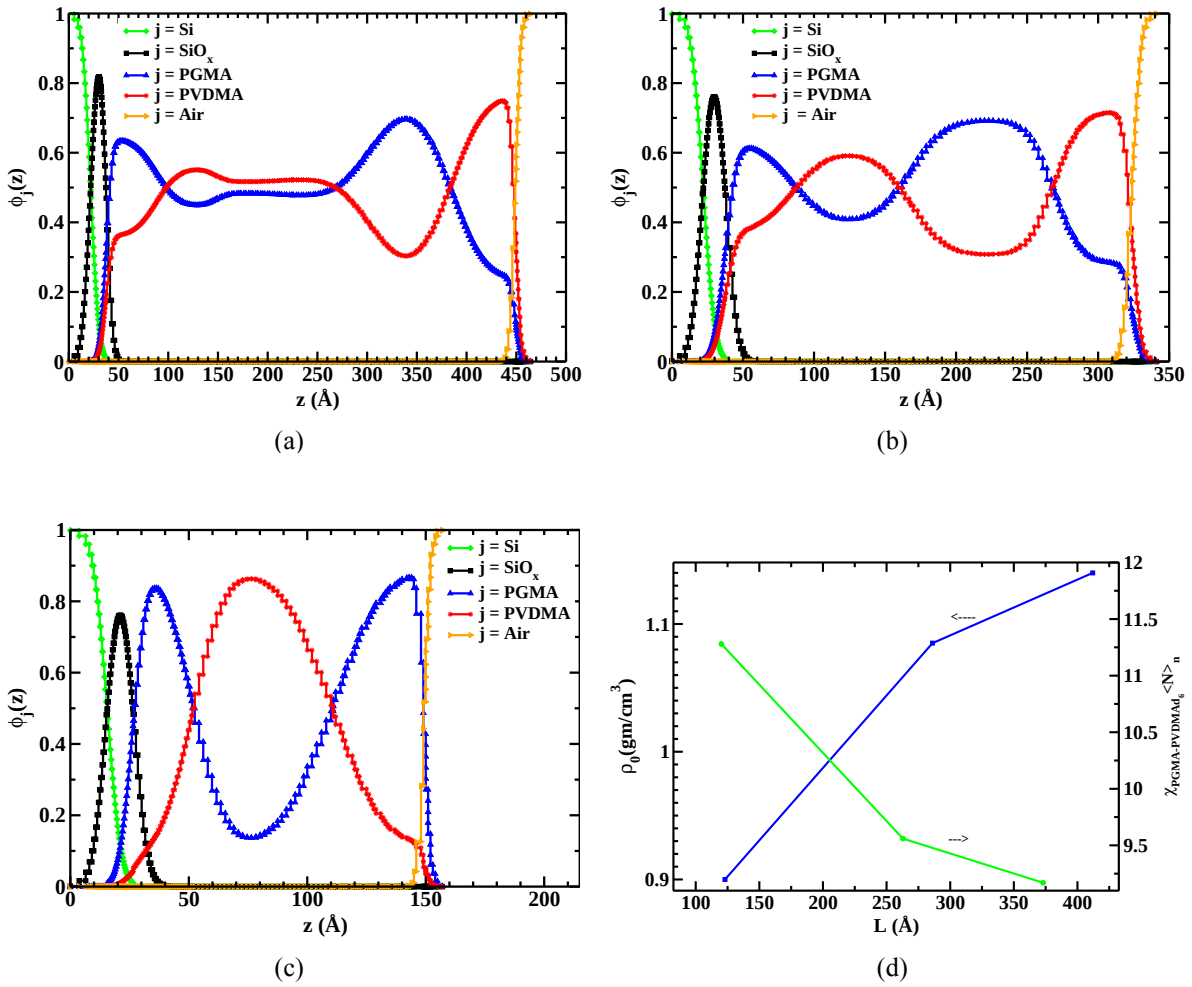

Figure 7: Volume fraction profiles of different components obtained using modeling of neutron reflectivity profiles for the three films of PGMA-PVDMA-d_6 di-block copolymers. Calculated reflectivity for these volume fraction profiles are shown as "best fits" in Figure 6.

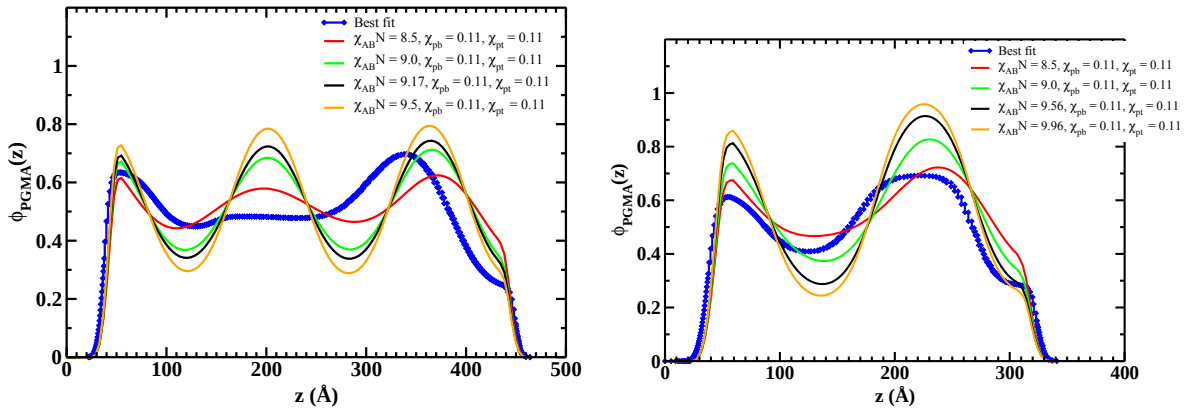

Figure 8: Comparison of volume fraction profiles obtained using modeling of neutron reflectivity profiles and simulations based on the SCFT for the three films of PGMA-PVDMA-d_6 di-block copolymers. Reflectivity profiles for these films and the best fits, which correspond to volume fraction profiles shown in blue above, are presented in Figure 6.

Conclusions

Coordinated theoretical and experimental studies are used to develop a fundamental understanding of microphase separation in thin films of lamellar-forming polydisperse di-block copolymers (a polydisperse PGMA block linked to a narrowly dispersed PVDMA-d_6 block). Theoretical investigations reveal that

a) Film thickness is shown to have important effects on microphase separation. Our field theoretic study reveals that entropic effects dominate systems having film thicknesses less than $5-6R_g$. It is shown that an increase in PDI of the polydisperse block induces conformational asymmetry, resulting in the polydisperse block having larger "effective" Kuhn segment length in comparison with the monodisperse block. The conformational asymmetry effects tend to drive the monodisperse block to the substrate. Also, the transition boundary for the number of packed lamellar domains shifts towards thicker films with an increase in PDI;

b) An increase in polydispersity index (PDI) of the polydisperse block (or PGMA) leads to an increase in lamellar domain spacing in the strong segregation limit and enhanced phase segregation in the weak segregation limit. Strong stretching theory reveals that this is a direct outcome of a

lower entropic penalty for stretching the polydisperse block with an increase in PDI. This is in agreement with earlier theoretical studies on such systems; and

c) Asymmetric polymer-substrate interactions lead to anti-symmetric lamellar morphology. For very thin films of thicknesses less than $5-6$ times the Gaussian radius of gyration, entropic effects compete against polymer-substrate interactions. In addition, monomer-monomer interactions affect sharpness of interfaces.

Our neutron reflectivity experiments and modeling of the reflectivity profiles using the theory reveals that

a) the SCFT provides a quantitative description of the density profiles and is a useful tool for modeling neutron reflectivity profiles.

b) the predictions of the theory are in quantitative agreement with the experiments.

c) for the thinnest film considered in this work, the polydisperse block (PGMA) lies near the silicon substrate, which shows that the PGMA-substrate interaction energy dominates over the entropy effects (resulting from induced conformational asymmetry).

As an outlook, we believe that prediction of neutron reflectivity profiles using the SCFT provides a facile and robust route for model verification and can be easily generalized to other polymeric systems near interfaces.

Materials and Methods

Polymer Synthesis and Characterization: The syntheses of 4,4-dimethyl-d6-2-vinyloxazolone ($VDMAd_6$) and PGMA-b-$PVDMAd_6$ by reversible addition fragmentation chain transfer (RAFT) polymerization are detailed in a previous report,[30] so only a brief summary of the polymerization is presented here. The diblock copolymer of poly(glycidylmethacrylate-block-vinyl-dimethylazlactone-d6), PGMA-b-$PVDMAd_6$, was made by chain extension of a PGMA macro-chain transfer agent (PGMA-macroCTA) made by RAFT polymerization of glycidylmethacrylate (GMA): $VDMAd_6$ ($2.18g, 1.50\times10^{2}$ mol) was combined with PGMA-macroCTA ($1.36g, 5.44\times10^{-5}$ mol; VDMA:PGMA-

macroCTA = 276), V-70 (5.59 mg; molar ratio of PGMA-macroCTA:AIBN = 3:1) and benzene (15.0 mL). The reaction vessel was capped with a rubber septum and the solution was sparged with dry argon for approximately 30 min. The reaction vessel was then placed in a heated oil bath thermostatted at 30° C and allowed to react for a predetermined time, after which the reaction vessel was immersed in liquid nitrogen to quench the polymerization. PGMA-b-PVDMA-d_6 was subsequently reconstituted in THF and precipitated in a 10-fold excess of hexanes (repeated 3 times) and dried in vacuo.

The recovered polymers were characterized by NMR spectroscopy and size exclusion chromatography (SEC). Solution $_1$H and $_{13}$C NMR spectroscopy was performed on a Varian VNMRS 500 MHz multinuclear spectrometer. Samples were placed in 5 mm-o.d. tubes with sample concentrations of 5 and 10% (w/v), respectively. Chloroform-d ($CDCl_3$) was used as the solvent and residual solvent peaks serve as internal standards. Molecular weights and polydispersities were obtained by SEC using a Waters Alliance 2695 Separations Module equipped with three Polymer Labs PLgel 5m mixed-C columns (300×7.5 mm) in series, a Waters Model 2414 Refractive Index detector ($\lambda = 880$ nm), a Waters Model 2996 Photodiode Array detector, a Wyatt Technology miniDAWN multi-angle light scattering (MALS) detector ($\lambda = 660$ nm), and a Wyatt Technology ViscoStar viscometer. THF was used as the mobile phase at a flow rate of 1 ml/min. The refractive index increment, dn/dc, was determined off-line and calculated using Astra V software, as described previously.[30]

Thin Film Assembly and Transmission Electron Microscopic (TEM) Characterization: Silicon samples (1.0×1.2 cm, Silicon Quest) were cleaned immediately before use by immersion for 90 minutes in a piranha acid solution at 110° C (3:1 v/v solution of sulfuric acid (EMD, 95-98%) and 30% hydrogen peroxide (VWR, 29-32%)) followed by rinsing with copious amounts of distilled, de-ionized water and drying with a stream of dry nitrogen. Thin films were made by the protocol described in our earlier work.[30] In short, silicon wafers were spin-coated (Laurell WS-400B-6NPP/LITE) with a solution of block copolymer (PGMA-b-PVDMA-d_6) in chloroform (2500 rpm, 15 s), and immediately annealed for 18 hr in an oven preheated to 110° C, which

provides chain mobility and allows the epoxide groups of PGMA to react with surface hydroxyls, thus anchoring the chains to the surface. After cooling under vacuum to room temperature, the modified wafers were immersed in chloroform and sonicated for 15 min to remove any physisorbed polymer from the surface, and then dried with a stream of dry, filtered N_2.

TEM characterizations were done using samples embedded in a low viscosity epoxy resin (Ted Pella) and microtomed into $\sim$ 75-nm-thick slices for experiments. Bright-field TEM imaging was performed in a Zeiss Libra 120 equipped with in-line energy filter. A low emission current of $\sim$4 μA and acceleration voltage of 120kV were used along with other proper beam conditions to carefully monitor and effectively minimize electron-dose introduced microstructural changes.

Neutron Reflectivity (NR): Measurements were made using the Spallation Neutron Source Liquids Reflectometer (SNS-LR) at Oak Ridge National Laboratory. The SNS-LR collects specular reflectivity data in continuous wavelength bands at several different incident angles. For the data presented here we used the wavelength bands ranging over 2.5 Å$< \lambda <$ 17 Åand measured reflectivity at discrete angles ranging over $0.6^\circ < \theta < 1.97^\circ$, thereby spanning a total wavevector transfer ($q = 4\pi \sin\theta/\lambda$) range of 0.008 Å$^{-1} < q <$ 0.16 Å^{-1}. Data were collected at each wavelength band and angle with incident-beam slits set to maintain a constant wavevector resolution of $\delta Q/Q = 0.03$, enabling data obtained at seven different (λ, θ) settings to be stitched together into a single reflectivity curve. To fit the data, the initial thicknesses measured using spectroscopic ellipsometry were used for reflectivity simulations and then these thicknesses were adjusted to correspond to the fringes in the neutron reflectivity. The neutron scattering length density (SLD) was determined using the equation SLD $= b/v$, where b is the monomer scattering length (sum of scattering lengths of constituent atomic nuclei) and v is the monomer volume. The calculated reflectivity curves were optimized for goodness-of-fit.

Small Angle Neutron Scattering: SANS data were collected at the Spallation Neutron Source of ORNL with the EQ-SANS instrument using the standard sample environment at ambient temperature.[35] The beam was collimated with a 25 mm source aperture and a 3 mm sample aperture. Three different instrument configurations were employed for the measurements: 7.0 m sample-to-

detector distance with a minimum wavelength setting of 10 Å; 4.0 m sample-to-detector distance with a minimum wavelength setting of 2.5 Å; and 1.3 m sample-to-detector distance with a minimum wavelength setting of 1.0 Å. In all configurations, the choppers were set to run at 60 Hz, thereby providing a single wavelength band of neutrons.[35] The samples were affixed in screw-together titanium cells having quartz windows for the measurements. An empty titanium sample cell was measured to provide a background to use during the reduction.

Data reduction into I(q) vs. q, where q is the neutron momentum transfer, followed standard procedures implemented in the MantidPlot software.[36] The data from the three configurations were merged into a single profile using the tool implemented in MantidPlot. The combined q-range provided by these three instrument configurations was $0.002\ \text{Å}^{-1} < q < 2.79\ \text{Å}^{-1}$. Data analysis was limited to fitting a Gaussian function to the observed diffraction peak using OriginPro (OriginLab Corp., Northamption, MA 01060, U. S. A.). The fitting utilized data from the 7.0 m and 4.0 m configurations described above. While the 1.3 m configuration did provide data in the range that included the diffraction peak, the q-resolution for that configuration is sufficiently broader (greater than 3 times as broad) than that of the other two configurations and not as well-characterized, making it prudent to not employ data from that configuration when fitting the diffraction peak.

Self-Consistent Field Theory (SCFT): SCFT for monodisperse and polydisperse di-block copolymer melts is very well-documented in literature. Details of our generalization of the SCFT for polydispers di-block copolymer melts to thin film geometry can be found in the Supporting Information.

Conflict of Interest: The authors declare no competing financial interest.

Acknowledgements: This research was conducted at the Center for Nanophase Materials Sciences, which is sponsored at Oak Ridge National Laboratory by the Scientific User Facilities Division, Office of Basic Energy Sciences, U.S. Department of Energy. SMKII acknowledges support from the National Science Foundation (Award No. 1133320). This research was sponsored by the Laboratory Directed Research and Development (LDRD) Program of Oak Ridge National Laborator (ORNL), and managed by UT-Battelle, LLC, for the U.S. Department of Energy.

Supporting Information: Details of the SCFT and algorithm used to solve non-linear equations can be found in the Supporting Information. This material is available free of charge *via* the internet

at `http://pubs.acs.org`.

References

1. Flory, P. *Principles of Polymer Chemistry*; Oxford University Press: Ithaca, 1953.

2. Burger, C.; Ruland, W.; Semenov, A. N. Polydispersity effects on the microphase-separation transition in block copolymers. *Macromolecules* **1990**, *23*, 3339–3346.

3. Fredrickson, G. H.; Sides, S. W. Theory of polydisperse inhomogeneous polymers. *Macromolecules* **2003**, *36*, 5415–5423.

4. Sides, S. W.; Fredrickson, G. H. Continuous polydispersity in a self-consistent field theory for diblock copolymers. *Journal of Chemical Physics* **2004**, *121*, 4974–4986.

5. Cooke, D. M.; Shi, A. C. Effects of polydispersity on phase behavior of diblock copolymers. *Macromolecules* **2006**, *39*, 6661–6671.

6. Matsen, M. W. Effect of large degrees of polydispersity on strongly segregated block copolymers. *European Physical Journal E* **2006**, *21*, 199–207.

7. Matsen, M. W. Polydispersity-induced macrophase separation in diblock copolymer melts. *Physical Review Letters* **2007**, *99*, 4.

8. Lynd, N. A.; Meuler, A. J.; Hillmyer, M. A. Polydispersity and block copolymer self-assembly. *Progress in Polymer Science* **2008**, *33*, 875–893.

9. Beardsley, T. M.; Matsen, M. W. Monte Carlo phase diagram for diblock copolymer melts. *European Physical Journal E* **2010**, *32*, 255–264.

10. Widin, J. M.; Schmitt, A. K.; Im, K.; Schmitt, A. L.; Mahanthappa, M. K. Polydispersity-induced stabilization of a disordered bicontinuous morphology in ABA triblock copolymers. *Macromolecules* **2010**, *43*, 7913–7915.

11. Beardsley, T. M.; Matsen, M. W. Monte Carlo Phase Diagram for a Polydisperse Diblock Copolymer Melt. *Macromolecules* **2011**, *44*, 6209–6219.

12. Widin, J. M.; Schmitt, A. K.; Schmitt, A. L.; Im, K.; Mahanthappa, M. K. Unexpected consequences of block polydispersity on the self-assembly of ABA triblock copolymers. *Journal of the American Chemical Society* **2012**, *134*, 3834–3844.

13. Schmitt, A. L.; Repollet-Pedrosa, M. H.; Mahanthappa, M. K. Polydispersity-driven block copolymer amphiphile self-assembly into prolate-spheroid micelles. *ACS Macro Letters* **2012**, *1*, 300–304.

14. Schmitt, A. L.; Mahanthappa, M. K. Polydispersity-driven shift in the lamellar mesophase composition window of PEO-PB-PEO triblock copolymers. *Soft Matter* **2012**, *8*, 2294–2303.

15. Widin, J. M.; Kim, M.; Schmitt, A. K.; Han, E.; Gopalan, P.; Mahanthappa, M. K. Bulk and thin film morphological behavior of broad dispersity poly(styrene-b-methyl methacrylate) diblock copolymers. *Macromolecules* **2013**, *46*, 4472–4480.

16. Li, Y.; Qian, H. J.; Lu, Z. Y.; Shi, A. C. Note: Effects of polydispersity on the phase behavior of AB diblock and BAB triblock copolymer melts: A dissipative particle dynamics simulation study. *Journal of Chemical Physics* **2013**, *139*, 2.

17. Matsen, M. W. Comparison of A-block polydispersity effects on BAB triblock and AB diblock copolymer melts. *European Physical Journal E* **2013**, *36*, 7.

18. Li, Y.; Qian, H. J.; Lu, Z. Y. The influence of one block polydispersity on phase separation of diblock copolymers: The molecular mechanism for domain spacing expansion. *Polymer* **2013**, *54*, 3716–3722.

19. Doi, M.; Edwards, S. F. *The Theory of Polymer Dynamics*; Clarendon Press: Oxford, 1986.

20. Fredrickson, G. H.; Ganesan, V.; Drolet, F. Field-Theoretic Computer Simulation Methods for Polymers and Complex Fluids. *Macromolecules* **2002**, *35*, 16–39.

21. Parratt, L. G. Surface studies of solids by total reflection of X-rays. *Physical Review* **1954**, *95*, 359–369.

22. Sinha, S. K.; Sirota, E. B.; Garoff, S.; Stanley, H. B. X-ray and neutron-scattering from rough surfaces. *Physical Review B* **1988**, *38*, 2297–2311.

23. Russell, T. P.; Karim, A.; Mansour, A.; Felcher, G. P. Specular reflectivity of neutrons by thin polymer-films. *Macromolecules* **1988**, *21*, 1890–1893.

24. Anastasiadis, S. H.; Russell, T. P.; Satija, S. K.; Majkrzak, C. F. Neutron reflectivity studies of the surface-induced ordering of diblock copolymer films. *Physical Review Letters* **1989**, *62*, 1852–1855.

25. Anastasiadis, S. H.; Russell, T. P.; Satija, S. K.; Majkrzak, C. F. The morphology of symmetric diblock copolymers as revealed by neutron reflectivity. *Journal of Chemical Physics* **1990**, *92*, 5677–5691.

26. Zhou, X. L.; Chen, S. H. Theoretical foundation of X-ray and neutron reflectometry. *Physics Reports-Review Section of Physics Letters* **1995**, *257*, 223–348.

27. Fredrickson, G. *The Equilibrium Theory of Inhomogeneous Polymers*; Clarendon Press: Oxford, 2006.

28. Mays, J. W.; Kumar, R.; Sides, S. W.; Goswami, M.; Sumpter, B. G.; Hong, K. L.; Wu, X. D.; Russell, T. P.; Gido, S. P.; Avgeropoulos, A. et al. Morphologies of poly(cyclohexadiene) diblock copolymers: Effect of conformational asymmetry. *Polymer* **2012**, *53*, 5155–5162.

29. Kumar, R.; Sides, S. W.; Goswami, M.; Sumpter, B. G.; Hong, K. L.; Wu, X. D.; Russell, T. P.; Gido, S. P.; Misichronis, K.; Rangou, S. et al. Morphologies of ABC Triblock Terpolymer Melts Containing Poly(Cyclohexadiene): Effects of Conformational Asymmetry. *Langmuir* **2013**, *29*, 1995–2006.

30. Lokitz, B. S.; Wei, J. F.; Hinestrosa, J. P.; Ivanov, I.; Browning, J. F.; Ankner, J. F.; Kilbey, S. M.; Messman, J. M. Manipulating Interfaces through Surface Confinement of Poly(glycidyl methacrylate)-block-poly(vinyldimethylazlactone), a Dually Reactive Block Copolymer. *Macromolecules* **2012**, *45*, 6438–6449.

31. Fredrickson, G. H.; Donley, J. P. Influence of broken conformational symmetry on the surface enrichment of polymer blends. *Journal of Chemical Physics* **1992**, *97*, 8941–8946.

32. Milner, S. T.; Witten, T. A.; Cates, M. E. Effects of polydispersity in the end-grafted polymer brush. *Macromolecules* **1989**, *22*, 853–861.

33. Turner, M. S. Equilibrium properties of a diblock copolymer lamellar phase confined between flat plates. *Physical Review Letters* **1992**, *69*, 1788–1791.

34. Fredrickson, G. H. Surface ordering phenomena in block copolymer melts. *Macromolecules* **1987**, *20*, 2535–2542.

35. Zhao, J. K.; Gao, C. Y.; Liu, D. The extended Q-range small-angle neutron scattering diffractometer at the SNS. *Journal of Applied Crystallography* **2010**, *43*, 1068–1077.

36. *Mantid (2013): Manipulation and Analysis Toolkit for Instrument Data.; Mantid Project;*, 2013. `http://dx.doi.org/10.5286/SOFTWARE/MANTID`.

Supporting Information: Thin films of lamellar forming polydisperse di-block copolymers

Rajeev Kumar,[*,†,‡] Bradley S. Lokitz,[¶] Scott W. Sides,[§] William Heller,[‖] John F. Ankner,[‖] Jim Browning,[‖] S. Michael Kilbey II,[⊥] and Bobby G. Sumpter[¶]

Computer Science and Mathematics Division, Oak Ridge National Lab, Oak Ridge, TN-37831, Center for Nanophase Materials Sciences, Oak Ridge National Lab, Oak Ridge, TN-37831, Center for Nanophase Materials Sciences,Oak Ridge National Laboratory, Oak Ridge, TN-37831, National Renewable Energy Laboratory, Golden, CO-80401, Spallation Neutron Source, Oak Ridge National Laboratory, Oak Ridge, TN-37831, and Department of Chemistry, University of Tennessee, Knoxville, TN-37996

E-mail: kumarr@ornl.gov

Self-Consistent Field Theory (SCFT) for confined polydisperse di-block copolymers

We consider a melt of *n* polydisperse di-block copolymer chains in between two parallel substrates. For comparison with neutron reflectivity experiments, one of the walls represents silicon substrate

[*]To whom correspondence should be addressed
[†]Computer Science and Mathematics Division, Oak Ridge National Lab, Oak Ridge, TN-37831
[‡]Center for Nanophase Materials Sciences, Oak Ridge National Lab, Oak Ridge, TN-37831
[¶]Center for Nanophase Materials Sciences,Oak Ridge National Laboratory, Oak Ridge, TN-37831
[§]National Renewable Energy Laboratory, Golden, CO-80401
[‖]Spallation Neutron Source, Oak Ridge National Laboratory, Oak Ridge, TN-37831
[⊥]Department of Chemistry, University of Tennessee, Knoxville, TN-37996

with a thin layer of silicon oxide (SiO_x) and the other represents polymer-air interface. We construct the partition function for this particular system by modeling interaction between polymers and substrates by short-range Flory's χ parameter approach.[1]

Representing the copolymer chains by continuous curves ($\vec{R}_\alpha(s)$ for α^{th} chain parameterized by the chain contour variable s), the Hamiltonian for the system is written as

$$H = \frac{3}{2b^2}\sum_{\alpha=1}^{n}\int_0^{N_\alpha} ds\left(\frac{d\vec{R}_\alpha(s)}{ds}\right)^2 + \rho_0^{-1}\int d\vec{r}\;\chi_{AB}\;\hat{\rho}_A(\vec{r})\hat{\rho}_B(\vec{r}) \quad (1)$$

$$+ \rho_0^{-1}\int d\vec{r}\sum_{k=t,b}\sum_{k'=A,B}\chi_{kk'}\;\rho_k(\vec{r})\hat{\rho}_{k'}(\vec{r}) \quad (2)$$

where the first term in H is the chain stretching entropy given by the so-called "Gaussian thread"[2] model for di-block chains with the same Kuhn segment legth for each block ($= b$). In this work, we have ignored *inherent* conformational asymmetry between the PGMA and PVDMA-d_6 blocks, which we have estimated to be negligible using approximate relations $b_k^3 \equiv v_k$, b_k and v_k being the Kuhn segment lengths and molar volume of monomer $k = PGMA, PVDMA - d_6$. Molar volumes for the PGMA and PVDMA-d_6 monomers are estimated using two different group contribution methods and these estimates are presented in Table 1.

The other terms represent interaction energy between different pairs within Flory-type model, which is parameterized by *dimensionless* χ_{ij} for species of kind i and j. $\rho_0 = \sum_{\alpha=1}^{n} N_\alpha/V$ is the total number density of monomers so that N_α is the polymerization index for chain α and V is the volume containing a finite amount of polymer chains. Later on, ρ_0 is used as a reference density to construct volume fraction profiles from number densities. Using the relation $\frac{\chi_{ij}}{\rho_0} = w_{ij} - \frac{w_{ii}+w_{jj}}{2}$ and $w_{ii} = \frac{1}{\kappa\rho_0^2}$, κ being isothermal compressibility, it turns out that $\chi_{ij} \sim 1/\rho_0$. Similar dependence of χ_{ij} parameter on the reference density (or volume) is postulated in its estimation using solubility parameters.

In Eq. 2, we have parameterized interaction energy between the monomers and particles in the substrates by χ parameters. Subscripts t, b are used to represent top and bottom substrate, respectively. For example, χ_{tA} represents the parameter for interaction between A monomer species

and the top substrate. Furthermore, regions where polymers interact with substrates are described by functions $\hat{\rho}_k(\vec{r})$ for $k = t, b$, which are taken to be hyperbolic tangent centered at each side of the polymer melt. Such an approach implicitly assumes that particle density inside the substrates is sufficiently large and continuous density profiles like $\rho_k(\vec{r})$ is an appropriate model for the interactions between particles in the substrate and monomers along the polymer chains.

The interaction parameters χ_{tA} and χ_{tB} determine tendencies for the polymer chains to either wet or be excluded from the confining surface. The relative sizes of the χ parameters determine the effective attraction or replusion for a monomer species to a wall species. For example, if $\chi_{tA} < \chi_{tB}$ then A monomers preferentially wet the surface wall. Absolute values of these parameters determine how strongly the monomers are repelled from the walls. The A/B monomer density operators and the substrate density functions[3,4] are

$$\hat{\rho}_A(\vec{r}) = \sum_{\alpha=1}^{n} \int_0^{N_{\alpha A}} ds\ \delta(\vec{r} - \vec{R}_\alpha(s)) \tag{3}$$

$$\hat{\rho}_B(\vec{r}) = \sum_{\alpha=1}^{n} \int_{N_{\alpha A}}^{N_\alpha} ds\ \delta(\vec{r} - \vec{R}_\alpha(s)) \tag{4}$$

$$\rho_b(\vec{r}) = \frac{\rho_0}{2}\left[1 - \tanh\left[\frac{z - z_b}{\xi_b}\right]\right] \tag{5}$$

$$\rho_t(\vec{r}) = \frac{\rho_0}{2}\left[1 + \tanh\left[\frac{z - z_t}{\xi_t}\right]\right] \tag{6}$$

where $N_{\alpha A}$ is the number of A monomers in α^{th} chain and z represents the co-ordinate perpendicular to substrates. z_k and ξ_k characterizes the location and width of polymer-substrate interfacial region, respectively, for $k = t, b$ representing the top and bottom substrates. Also, the choice of so called masking functions (cf. Eqs. 5- 6) fixes the origin of the coordinate system at the bottom substrate and places the top substrate on the positive z-axis. Furthermore, for comparison with set-up for neutron reflectivity experiments, the top substrate represents polymer-air interface and the bottom substrate represents polymer-silicon interface with thin layer of silicon oxide sandwiched between them. Note that the SCFT presented here takes the masking functions as an input. For a refined comparison with the neutron reflectivity experiments on the volume fraction profiles in

the interior of films, we obtain these functions by *a posteriori* analysis of reflectivity profiles as detailed in the next section.

The partition function for this system can be written as

$$Z = \int \prod_{\alpha=1}^{n} D\left[\vec{R}_\alpha\right] \exp\left[-H\right] \prod_{\mathbf{r}} \delta[\rho_0 - \sum_{k=t,b} \rho_k(\vec{r}) - \hat{\rho}_A(\vec{r}) - \hat{\rho}_B(\vec{r})] \tag{7}$$

The delta function enforces an incompressibility constraint among A monomers, B monomers and the substrates such that the total monomer density is kept constant. A field theory can be constructed using standard particle to field transformations, which leads to (cf. Eq. 7)

$$Z = \int D[\rho_A] D[\rho_B] D[\omega_A] D[\omega_B] D[p] \; e^{-\beta F} \tag{8}$$

where $\rho_{k=A,B}(\mathbf{r})$ represents collective density variable and $w_{k=A,B}(\mathbf{r})$ is the conjugate field introduced through the exponential representation of the delta functional $\delta[\rho - \hat{\rho}]$. p is the Lagrange's multiplier which enforces incompressibility constraint. Explicitly, βF is given by

$$\begin{aligned} \beta F = & \int d\vec{r} \left[\rho_0^{-1} (\chi_{AB} \rho_A(\mathbf{r}) \rho_B(\mathbf{r}) + \sum_{k=t,b} \sum_{k'=A,B} \chi_{kk'} \rho_k(\mathbf{r}) \rho'_k(\mathbf{r})) - i w_A(\mathbf{r}) \rho_A(\mathbf{r}) - i w_B(\mathbf{r}) \rho_B(\mathbf{r}) \right. \\ & \left. - i p(\mathbf{r}) (\rho_0 - \sum_{k=t,b} \rho_k(\mathbf{r}) - \rho_A(\mathbf{r}) - \rho_B(\mathbf{r})) \right] - \sum_{\alpha=1}^{n} \ln Q_\alpha[i w_A, i w_B; N_\alpha] \end{aligned} \tag{9}$$

where $Q_\alpha[i w_A, i w_B; N_\alpha]$ is the single-chain partition function for α^{th} chain, given by

$$Q_\alpha = \frac{\int D\left[\vec{R}_\alpha\right] \; \exp\left\{ -\frac{3}{2b^2} \int_0^{N_\alpha} ds \left(\frac{\partial \vec{R}_\alpha(s)}{\partial s} \right)^2 - \int_0^{N_{\alpha A}} ds \; i w_A(\vec{R}_\alpha(s)) - \int_{N_{\alpha A}}^{N_\alpha} ds \; i w_B(\vec{R}_\alpha(s)) \right\}}{\int D\left[\vec{R}_\alpha\right] \; \exp\left\{ -\frac{3}{2b^2} \int_0^{N_\alpha} ds \left(\frac{\partial \vec{R}_\alpha(s)}{\partial s} \right)^2 \right\}} \tag{10}$$

The equation for Q_α is analogous to the Feynman-Kac formula in the path-integral description of

quantum mechanics[5] and may be expressed as

$$Q_\alpha = V^{-1} \int d\vec{r}\, q_\alpha(\vec{r}, N_\alpha) \tag{11}$$

where $q_\alpha(\vec{r}, s)$ is a restricted chain partition function that may be calculated as the solution to the modified diffusion equation

$$\frac{\partial q_\alpha(\vec{r}, s)}{\partial s} = \begin{cases} \frac{b^2}{6}\nabla^2 q_\alpha(\vec{r}, s) - i w_A(\vec{r}) q_\alpha(\vec{r}, s), & 0 < s < N_{\alpha A} \\ \\ \frac{b^2}{6}\nabla^2 q_\alpha(\vec{r}, s) - i w_B(\vec{r}) q_\alpha(\vec{r}, s), & N_{\alpha A} < s < N_\alpha \end{cases} \tag{12}$$

subject to the initial condition $q_\alpha(\vec{r}, 0) = 1$.

Evaluation of discrete sum in Eq. 9 for polydisperse block copolymers is computationally extensive. In order to evaluate the sum, we approximate it by an integral over continuous chain length distribution as discussed in the next section.

Modeling polydispersity effects by continuous chain length distribution

In order to model di-block copolymers containing polydisperse A block and monodisperse B block, we assume that the A block has the chain-length distributed as per the *normalized* Schulz-Zimm distribution[1,6–8] given by

$$p_A(N) = \left(\frac{N}{N_A}\right)^{\nu-1} \frac{\exp\left[-N/N_A\right]}{N_A \Gamma(\nu)} \tag{13}$$

where Γ is the Gamma function.

For the distribution, the number average, weight average and polydispersity index of A block is given by $\nu N_A, (\nu+1)N_A$ and $(\nu+1)/\nu$, respectively. Assuming that the B block is monodisperse with fixed degree of polymerization ($= N_B$), it is straightforward to compute the polydispersity of the $A-B$ di-block in terms of ν, N_A and N_B. Also, the chain length distribution for the $A-B$

di-block is $p_{AB}(N') = p_A(N')$ for $N' < (N - N_B)$ and $p_{AB}(N') = 0$ otherwise. Using the continuous chain length distribution, discrete sum over chain index α in Eq. 9 can be replaced by integrals over chain lengths via $\frac{1}{n}\sum_{\alpha=1}^{n} \ln Q_\alpha[iw_A, iw_B; N_\alpha) = \int_0^\infty dN\, p_{AB}(N) \ln Q[iw_A, iw_B; N]$.

The field theoretic transformations and approximation of continuous chain length distribution lead to deconvolution of chain-chain interactions into single chain problem, where each chain interacts with fields w_k. Even with these simplifications, numerical evaluation of the functional integrals in Eqn. 8 poses a serious challenge. In the following, we approximate these integrals by saddle-point approximation so that the full partition function is approximated by its value when the fields attain their "saddle-point" values. Noting that the saddle-points are located along the imaginary axis in the complex-w plane,[3,9] we rescale these fields by writing $\omega_A = i \langle N \rangle_n w_A$, $\omega_B = i \langle N \rangle_n w_B$, and $\eta = i \langle N \rangle_n p$ so that ω_A, ω_B and η are purely real and $\langle N \rangle_n = \nu N_A + N_B$ is the number average chain length for the di-block copolymers. Also, volume fractions are defined by $\phi_k(\vec{r}) = \rho_k(\vec{r})/\rho_0$ for $k = A, B, t, b$.

The value of the fields [ϕ_A,ϕ_B,ω_A,ω_B,η] at the saddle-point satisfy the following set of equations

$$\omega_A(\vec{r}) = \chi_{AB} \langle N \rangle_n \, \phi_B(\vec{r}) + \sum_{k=t,b} \chi_{kA} \langle N \rangle_n \phi_k(\vec{r}) + \eta(\vec{r}) \tag{14}$$

$$\omega_B(\vec{r}) = \chi_{AB} \langle N \rangle_n \, \phi_A(\vec{r}) + \sum_{k=t,b} \chi_{kB} \langle N \rangle_n \phi_k(\vec{r}) + \eta(\vec{r}) \tag{15}$$

$$\phi_A(\vec{r}) + \phi_B(\vec{r}) = 1 - \sum_{k=t,b} \phi_k(\vec{r}) \tag{16}$$

$$\phi_A(\vec{r}) = \int_0^\infty dN \frac{p_{AB}(N)}{Q\{N/\langle N \rangle_n\}} \int_0^{(N-N_B)/\langle N \rangle_n} d\bar{s}\, q(\vec{r}, \bar{s})\, q^\dagger(\vec{r}, \bar{s}) \tag{17}$$

$$\phi_B(\vec{r}) = \int_0^\infty dN \frac{p_{AB}(N)}{Q\{N/\langle N \rangle_n\}} \int_{(N-N_B)/\langle N \rangle_n}^{N/\langle N \rangle_n} d\bar{s}\, q(\vec{r}, \bar{s})\, q^\dagger(\vec{r}, \bar{s}) \tag{18}$$

where

$$Q = V^{-1} \int d\vec{r}\, q(\vec{r}, N/\langle N \rangle_n) \tag{19}$$

and we have used $\rho_0 = n\langle N\rangle_n / V$ along with a well-known factorization of the single-chain path integral[5,10,11] in writing Eqns. 17 and 18. Furthermore, solution to the restricted partition function $q^\dagger$, may be calculated as the solution to a modified diffusion equation similar to Eqn. 12 subject to the initial condition $q^\dagger(\vec{r}, s = N/\langle N\rangle_n) = 1$.[12]

We have solved the set of equations representing saddle-point in the complex plane using an iterative procedure devised by Drolet and Fredrickson[9,13] (so called "model A" type relaxation dynamics[14]). This results in the following expressions for updating the chemical potential fields from relaxation step n to $n+1$

$$\begin{aligned} \omega_A^{n+1} - \omega_A^n &= \lambda' \frac{\delta\beta F}{\delta\phi_B^n} + \lambda \frac{\delta\beta F}{\delta\phi_A^n} \\ &= \lambda' \left[\chi_{AB} \langle N\rangle_n \phi_A^n + \sum_{k=t,b} \chi_{kB} \langle N\rangle_n \phi_k - \omega_B^n + \eta^n \right] \\ &+ \lambda \left[\chi_{AB} \langle N\rangle_n \phi_B^n + \sum_{k=t,b} \chi_{kA} \langle N\rangle_n \phi_k - \omega_A^n + \eta^n \right] \end{aligned} \tag{20}$$

Similar equation is used for relaxing ω_B is written as

$$\omega_B^{n+1} - \omega_B^n = \lambda \frac{\delta\beta F}{\delta\phi_B^n} + \lambda' \frac{\delta\beta F}{\delta\phi_A^n} \tag{21}$$

where the relaxation parameters are chosen such that $\lambda' < \lambda$ and $\lambda > 0$ and the quantities ϕ_A^n, ϕ_B^n are calculated as functionals of ω_A^n, ω_B^n using their expression in terms of q and $q^\dagger$. For the evaluation of integrals over the chain lengths in Eqs. 17 and 18, we have used the Gaussian quadrature scheme applied to the polydisperse di-block copolymer melts in Ref.[7] For the results presented in this work, we have found ten quadrature points to be sufficient to provide converged results on the volume fraction profiles due to the fact that most of the calculations done in this work lies in the weak segregation limit. For some of our test runs done in the intermediate and strong segregation, we have found that more number of quadrature points are required.

The pressure field is updated using the expression

$$\eta^{n+1} = \frac{1}{2}\left[\omega_A^{n+1} + \omega_B^{n+1} - \chi_{AB}\langle N\rangle_n + (\chi_{AB} - \sum_{k=t,b}\{\chi_{kA} + \chi_{kB}\})\langle N\rangle_n \phi_k\right] \quad (22)$$

After updating the pressure field, its spatial average $V^{-1}\int \eta(\vec{r})\, d\vec{r}$ is subtracted so as to improve the algorithm's stability. This has no effect on the equilibrium structure of the chains as the thermodynamic properties are invariant to a constant shift in the pressure field. With the new fields ω_A, ω_B and η the procedure is repeated until the saddle-point configurations are found.

Interpretation of neutron reflectivity profiles

As mentioned in the main text, for the interpretation of neutron reflectivity profiles, we have we have followed a three step procedure. In the first step, an initial estimate for the film thickness was obtained using fringes in the neutron reflectivity data. For these film thicknesses, the SCFT simulations with the hyperbolic tangent masking functions (as discussed in the previous section) were used to determine the number of strata that can be packed. These simulations were run to mimic PGMA-b-PVDMA-d_6 systems with $\mathrm{PDI}_{PGMA} = 1.36$ and different values of χ parameters characterizing polymer-polymer and polymer-substrate interactions. In the second step, a multi-layer model based on the number of strata and density profiles was constructed to fit the neutron reflectivity data using Parratt's formalism. In other words, we have used predictions of the SCFT as a starting guess for the construction of multi-layer models, which makes it easier to find the best fit. Note that the SCFT provides description of density profiles at equilibrium in the thin films. However, it is not clear whether the multi-layer models corresponding to the best fits represent equilibrium or non-equilibrium structure due to the presence of kinetic effects in thin films. In order to better understand non-equilibrium effects, we have taken the third step where we extract "refined" masking functions and total film thicknesses from the best fits obtained using the two steps mentioned above and use them to run another round of SCFT simulations. In order to obtain the volume fraction profiles from the SLD profiles for the best fits, we used the relation $SLD(\mathbf{r}) =$

$\sum_{k=GMA,VDMA-d_6} SLD_k \rho_k(\mathbf{r})/\rho_0$, where SLD_k and ρ_k represent SLD and number density of the monomer of type k, respectively. Monomeric SLDs were computed using the molecular formula and ρ_0. Furthermore, ρ_0 was varied to make sure that spatial average of $\rho_k(\mathbf{r})/\rho_0$ is 0.5 for the three samples studied in this work. Volume fraction profiles obtained in this way representing the best fits for the neutron reflectivity data are compared with the profiles obtained from the SCFT simulations.

We have varied five χ parameters to change the volume fraction profiles inside the film. Due to the fact that each SCFT calculation is computationally extensive and takes around four hours to obtain converged density profiles on eight cores in parallel execution, it is not practical to vary the five χ parameters. As it turns out that the polydisperse di-block studied in this work lies in the weak and intermediate segregation limit. So, we have estimated the χ parameters using an analytical theory in the weak segregation limit.[15] The theory is a straightforward generalization from the case of monodisperse copolymers to polydisperse. Details of the theory will be presented elsewhere. Volume fraction profiles obtained from the modeling of neutron reflectivity data can be readily fitted with the predicted functional form in the so-called "ordered bulk" regime, in parlance of Ref.[15] For these fits, each substrate is assumed to behave independent of each other. The fits are shown in Fig. Figure 2. From the fit parameters, $\chi_{PGMA-PVDMAd_6} \langle N \rangle_n$ is computed and presented in the main text. Furthermore, the stability limit and characteristic length scale appearing at the stability limit of disordered phase in the polydisperse case have already been presented in the literature and we have reproduced those results as shown in Fig. Figure 3.

References

1. Flory, P. *Principles of Polymer Chemistry*; Oxford University Press: Ithaca, 1953.
2. Doi, M.; Edwards, S. F. *The Theory of Polymer Dynamics*; Clarendon Press: Oxford, 1986.
3. Fredrickson, G. *The Equilibrium Theory of Inhomogeneous Polymers*; Clarendon Press: Oxford, 2006.

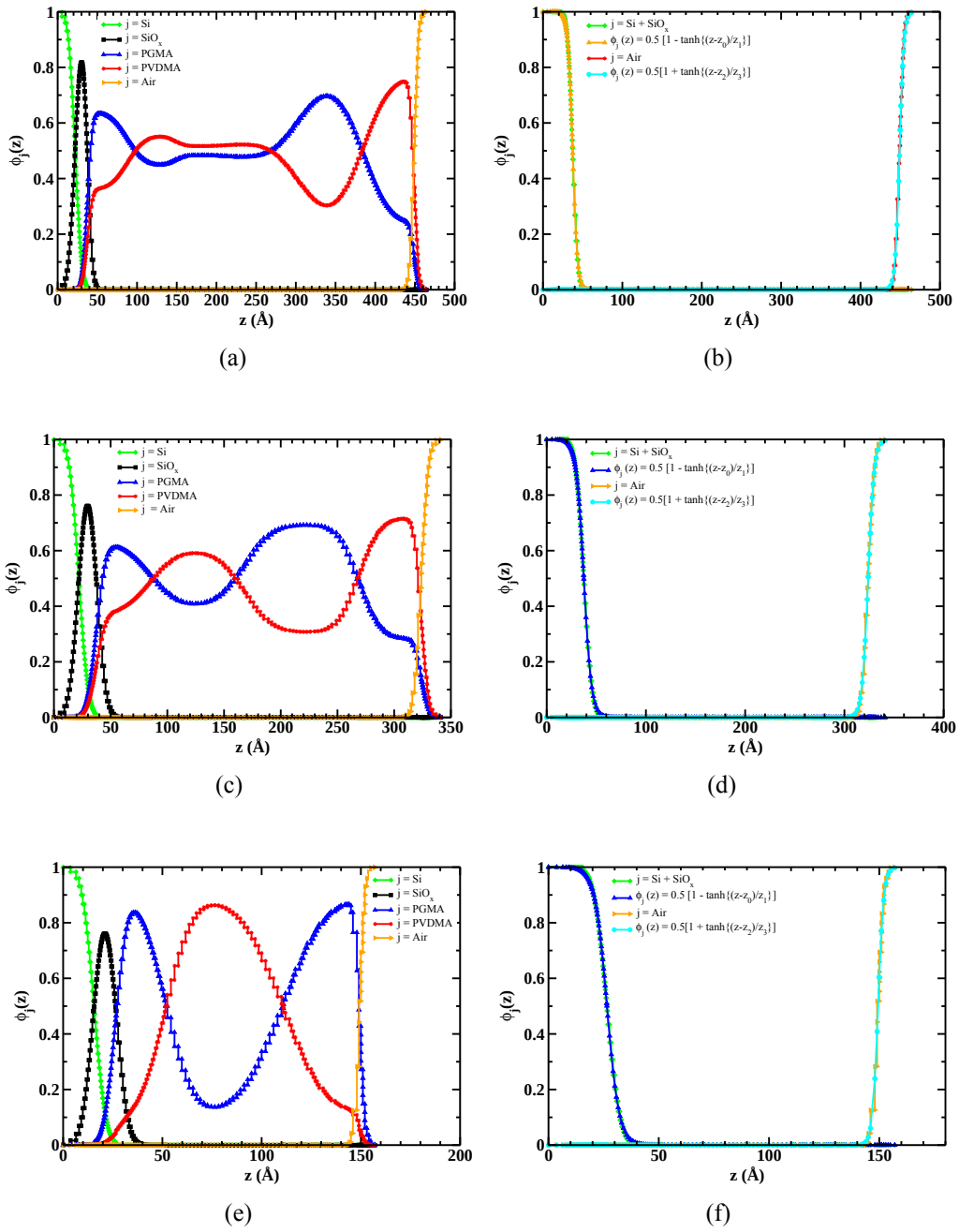

Figure 1: Extraction of masking functions from the muli-layer model corresponding to the best fit of neutron reflectivity profile for the three samples is described here. Figure (a),(c) and (e) shows the volume fraction profiles of different components used in the multi-layer model. As the SCFT model doesn't distinguish between the silicon and its oxide layer, the masking function near these substrates represents combined effects of these. In order to extract the masking functions, volume fractions of silicon and oxide layer on it are added in Figure (b),(d) and (f); functions based on hyperbolic tangents are used to fit the volume fraction of air and silicon-silicon oxide layers. These masking functions are used to run the SCFT simulations with different values of five χ parameters.

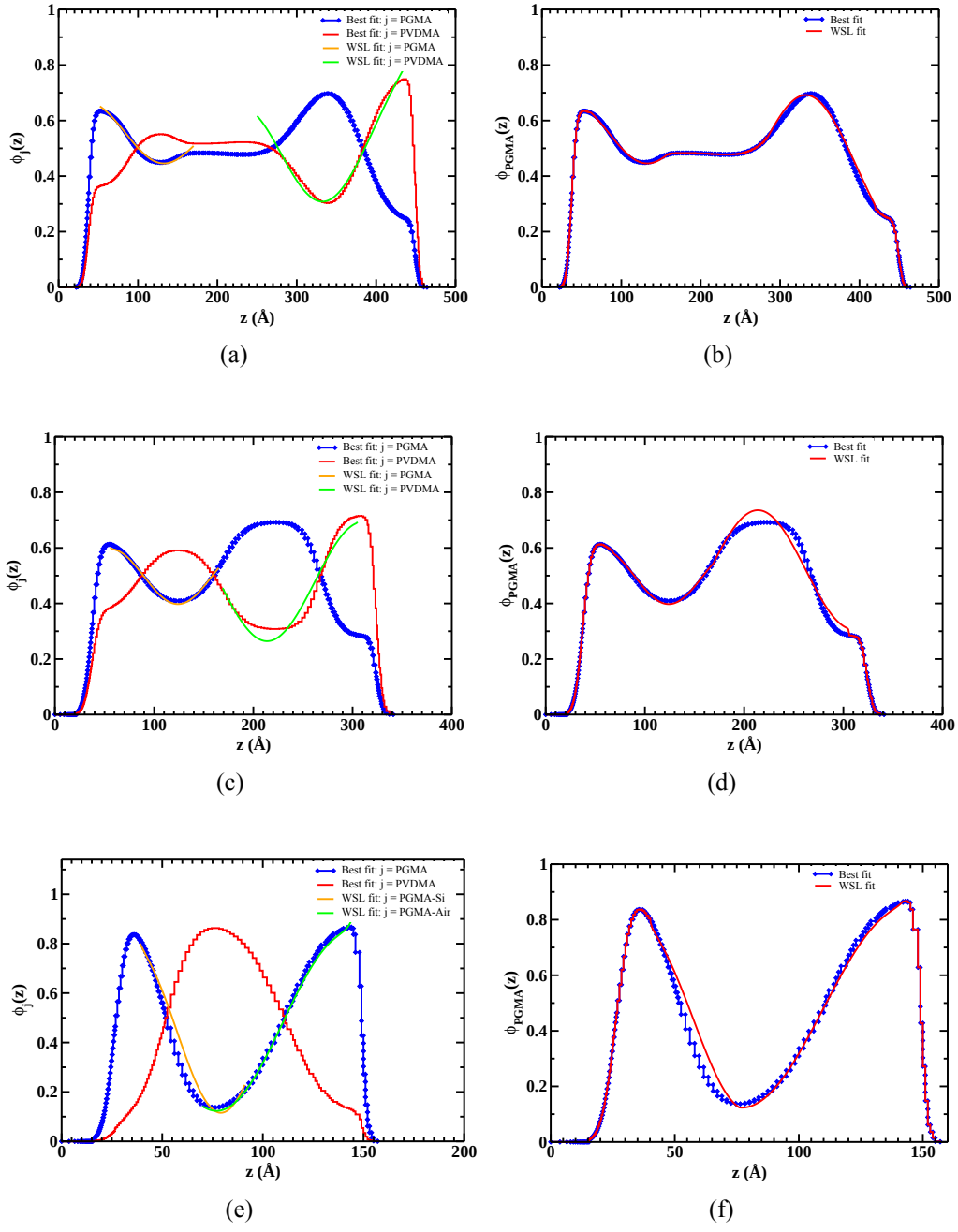

Figure 2: Procedure for extracting the χ parameters from the volume fraction profiles corresponding to best fits of neutron reflectivity profiles for three films of PGMA-PVDMA-d_6 di-block copolymers is described here. Top, middle and bottom figures correspond to films with total thicknesses of $45, 34$ and 15 nm, respectively. Left figures show the fits to the volume fraction profiles to analytical profiles and the right figures show the volume fraction profiles after the addition of masking functions. For the thickest films, flat region in the interior of the film can not be modeled by the analytical profiles and is kept the same in obtaining the figure on the right hand side.

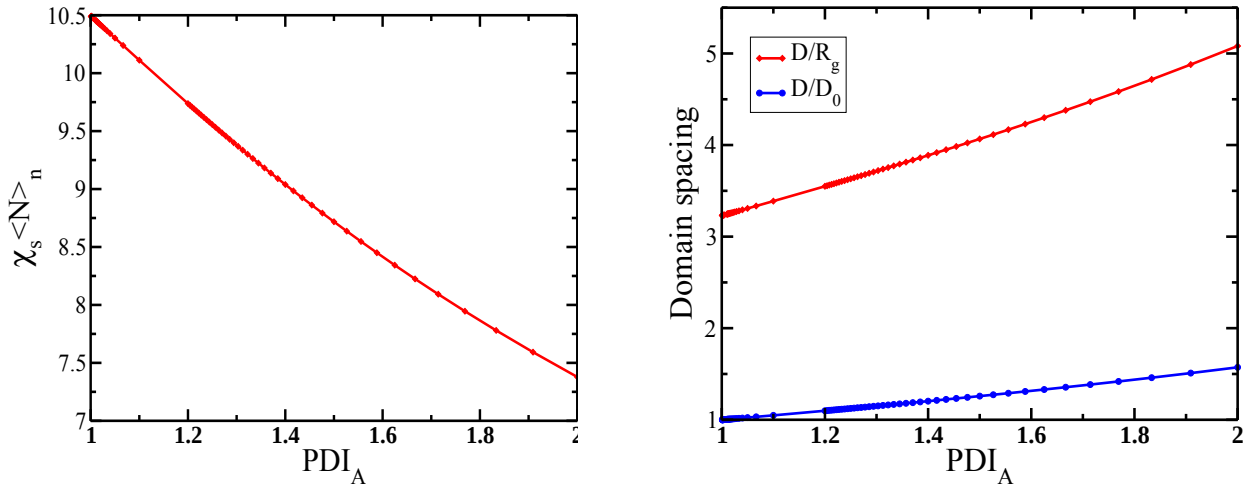

Figure 3: Characteristics of the stability limit and characteristic domain spacing in polydisperse di-block copolymers as predicted by the weak segregation theory.

4. Matsen, M. W. Thin films of block copolymer. *Journal of Chemical Physics* **1997**, *106*, 7781–7791.

5. Feynman, R. P.; Hibbs, A. R. *Quantum Mechanics and Path Integrals*; McGraw-Hill Book Company: New York, 1965.

6. Fredrickson, G. H.; Sides, S. W. Theory of polydisperse inhomogeneous polymers. *Macromolecules* **2003**, *36*, 5415–5423.

7. Sides, S. W.; Fredrickson, G. H. Continuous polydispersity in a self-consistent field theory for diblock copolymers. *Journal of Chemical Physics* **2004**, *121*, 4974–4986.

8. Lynd, N. A.; Meuler, A. J.; Hillmyer, M. A. Polydispersity and block copolymer self-assembly. *Progress in Polymer Science* **2008**, *33*, 875–893.

9. Fredrickson, G. H.; Ganesan, V.; Drolet, F. Field-Theoretic Computer Simulation Methods for Polymers and Complex Fluids. *Macromolecules* **2002**, *35*, 16–39.

10. Freed, K. F. Functional Integrals and Polymer Statistics. *Adv. Chem. Phys.* **1972**, *22*, 1.

11. Helfand, E. Theory of inhomogeneous polymers: Fundamentals of the Gaussian random-walk model. *J. Chem. Phys.* **1974**, *62*, 999–1005.

12. Matsen, M. W.; Schick, M. Stable and Unstable Phases of a Diblock Copolymer Melt. *Phys. Rev. Lett.* **1994**, *72*, 2660–2663.

13. Drolet, F.; Fredrickson, G. H. Combinatorial Screening of Complex Block Copolymer Assembly with Self-Consistent Field Theory. *Phys. Rev. Lett.* **1999**, *83*, 4317–4320.

14. Hohenberg, P. C.; Halperin, B. I. Theory of dynamic critical phenomena. *Rev. Mod. Phys.* **1977**, *49*, 436–475.

15. Fredrickson, G. H. Surface ordering phenomena in block copolymer melts. *Macromolecules* **1987**, *20*, 2535–2542.